Supplementary Information

Toughening hydrogel through multiscale hydrogen bonding network enabled by saccharides for bio-machine interface

Yuhang Ye[a], Xun Niu[b], Kelvin Zheng[a], Zhangmin Wan[b], Wucheng Zhang[d], Qi Hua[c], Jiaying Zhu[a], Zhe Qiu[a], Siheng Wang[e], He Liu[e], Scott Renneckar[c], Orlando Rojas[b], Feng Jiang[a, *]

[a]Sustainable Functional Biomaterials Lab, Department of Wood Science, University of British Columbia, 2900 – 2424 Main Mall, Vancouver, BC V6T 1Z4, Canada.

[b]Department of Chemical & Biological Engineering, Department of Chemistry and Department of Wood Science, The University of British Columbia, 2360 East Mall, Vancouver, BC V6T 1Z3, Canada.

[c]Advanced Renewable Materials Lab, Faculty of Forestry, The University of British Columbia, Vancouver, BC V6T 1Z4, Canada.

[d]Department of Physics, Princeton University, Jadwin Hall, Princeton, NJ 08540, United States.

[e]Institute of Chemical Industry of Forestry Products, Chinese Academy of Forestry, Nanjing, Jiang Su province, 210042, China

Text S1. Details about Gaussian-based learning model and dynamic molecular simulation.

Figure S1. The change of number of hydrogen bonds of varied systems within 100 ns.

Figure S2. Typical tensile stress-strain curves of g-PAM/CNF hydrogels with varied CNF contents.

Figure S3. Enhancement factor comparison of different hydrogel systems, using pure PAM hydrogels as reference.

Figure S4. Typical tensile stress-strain curves of hydrogels with varied components.

Figure S5. Swelling kinetic curves of PAM hydrogel soaking water and glucose/CNF bath

Figure S6. Typical tensile stress-strain curves of hydrogels fabricated by post swelling method.

Figure S7. Tensile curve of notched g-PAM/CNF hydrogel sample and testing photo

Figure S8. Mechanical properties of pristine PAM-gelatin double network hydrogels and after being strengthened by multiscale hydrogen bonding strategy，including (a) Tensile stress-strain curves; (b) Stress; (c) Strain; and (d) Work of fracture.

Figure S9. Mechanical properties of pristine PVA hydrogels and after being strengthened by multiscale hydrogen bonding strategy，including (a) Tensile stress-strain curves; (b) Stress; (c) Strain; and (d) Work of fracture.

Figure S10. (a) EIS Nyquist curves of varied hydrogel systems; (b)Calculated ionic conductivity of different hydrogel systems.

Figure S11. (a) EIS Nyquist curves and (b) ionic conductivity value of g-PAM/CNF hydrogels at 25 and -8 ^{o}C

Figure S12. Digital photos presenting the appearance and mechanical properties change for PAM and g-PAM/CNF hydrogels at - 8 ^{o}C.

Figure S13. DSC profiles for a series of hydrogel systems.

Figure S14. 1H NMR spectra for a series of hydrogel systems.

Figure S15. Digital photos demonstrating the appearance change of PAM and g-PAM/CNF hydrogels after being exposed to ambient conditions for 48 hrs

Figure S16. Typical tensile stress-strain curves of g-PAM/CNF alchogels curves with different CNF contents.

Figure S17. Optical microscopic photos demonstrating the color change of g-PAM/CNF alcogels under different strains (under polarizer).

Figure S18. Machine learning models for building continuous relationship among (a) CIE X, (b)Y value, and corresponding strain with specified error bar.

Figure S19. (a) Representative force/width vs. displacement curves for the 180-degree peel tests of various hydrogels; (b) corresponding calculated interfacial toughness value (the inserted photo showing the strong adhesion between g/PAM-CNF hydrogel and porcine skin).

Figure S20. EMG signal recorded by electrode without hydrogel as adhesive

Gaussian process-based machine learning model

We applied the Gaussian process from Python and scikit-learn to extrapolate the relationship between the stretch of the sample and its color in XY color space. Gaussian process is a regression method that turns discrete data with uncertainty into a collection of continuous random variables such that the joint distribution of every finite subset of random variables is multivariate Gaussian, whose mean and covariance are determined by the kernels. We chose the kernel to be the linear combination of RBF kernel and Gaussian white noise kernel and tuned the parameters of the kernel to maximize the marginal likelihood. Based on the probability distribution of the random variables, we evaluated the relationship between stretch and color with appropriately estimated uncertainty. The code script used is attached below,

```
# install packages and data
from sklearn.gaussian_process import GaussianProcessRegressor
from sklearn.gaussian_process.kernels import RBF, WhiteKernel
from sklearn.gaussian_process.kernels import Matern
import numpy as np

X_train = np.array([0.332479005,0.495598305,0.404865431,0.195275658,0.269449602]).reshape(-1, 1)
Y_train = np.array([0.312865344,0.452977701,0.231988688,0.197569236,0.36189377]).reshape(-1, 1)
t_train = np.array([0.00,1.00,1.50,2.00,2.50]).reshape(-1, 1)

t = np.linspace(0, 2.5, 100, endpoint=True).reshape(-1, 1)

# build up the model
kernel = 1*RBF(length_scale=1e1, length_scale_bounds=(1e-2, 1)) + WhiteKernel(
    noise_level=5e-4, noise_level_bounds=(1e-5, 5e-4)
)

gpr1 = GaussianProcessRegressor(kernel=kernel, alpha=0.0)
```

```
gpr1.fit(t_train, X_train)
X_mean, X_std = gpr1.predict(t, return_std=True)

gpr2 = GaussianProcessRegressor(kernel=kernel, alpha=0.0)
gpr2.fit(t_train, Y_train)
Y_mean, Y_std = gpr2.predict(t, return_std=True)

import matplotlib.pyplot as plt

_ = plt.title(
    f"Initial: {kernel}\nOptimum: {gpr1.kernel_}\nLog-Marginal-Likelihood: "
    f"{gpr1.log_marginal_likelihood(gpr1.kernel_.theta)}",
    fontsize=8,
)
plt.plot(t, X_mean, "-", ms=5, label="mean")
plt.fill_between(t[:,0], X_mean[:,0] + X_std, X_mean[:,0] - X_std, alpha=0.4, label="std")
plt.plot(t_train,X_train,"o",label="data")
plt.legend();

_ = plt.title(
    f"Initial: {kernel}\nOptimum: {gpr2.kernel_}\nLog-Marginal-Likelihood: "
    f"{gpr2.log_marginal_likelihood(gpr2.kernel_.theta)}",
    fontsize=8,
)
plt.plot(t, Y_mean, "-", ms=5, label="mean")
plt.fill_between(t[:,0], Y_mean[:,0] + Y_std, Y_mean[:,0] - Y_std, alpha=0.4, label="std")
plt.plot(t_train,Y_train,"o",label="data")
plt.legend();

ax = plt.axes(projection='3d')
ax.scatter3D(X_train[:,0], Y_train[:,0], t_train[:,0])
```

```
ax.plot3D(X_mean[:,0], Y_mean[:,0], t[:,0], 'gray')
ax.view_init(10, 60)
```

Molecular dynamic stimulation

***Classical* molecular dynamics simulation (CMD)**

The cellulose Iβ crystallite was constructed according to the crystallographic vector.[2] The PAM molecules with 20 repetition unit were made by chamm-gui, polymer builder.[3] In addition, the configuration of complex structure was built by using PACKMOL.[4] Visualization and analysis of MD trajectories were carried out with the VMD package (version 1.9.3).[5] All the MD simulations described herein were conducted by using Gromac,[6] version 2021.6, with the CHARMM36 Force Field for carboxylate and PAM molecules and TIP3P water model3.[7,8] Firstly, all the configurations were undergone energy minimization by using both steep descents and followed conjugated gradient methods. The process was carried out in NPT ensemble at 303.15 K and 1 bar ambient pressure for 1 ns simulation to equilibrate. Subsequently, the production simulation was carried out in NPT ensemble for another 100 ns. During all the simulations, the particle mesh Ewald approach was used to evaluate long-range electrostatic interaction. A real space cutoff of 1.2 nm and Lennard-Jones interaction cutoff of 1.2 nm was used. The Potential-Shift-Verlet scheme and force-switch function were used to modify the electrostatic interaction and Lennard-Jones interaction reach the smooth transition effect at the cutoff. [7,8] Gmx utility was used to analyze the hydrogen bonds and non-bonded interaction. The cut-off criteria to determine the hydrogen bonds is 30 degree for angle and 0.35 nm for distance.

Non-covalent interaction calculation

To gain more details of non-covalent interaction, Symmetry-Adapted Perturbation Theory (SAPT) was used to analyze the interaction energy between the molecules used in the previous CMD. All the structures (including cellulose, water, and PAM molecules) herein were optimized by using Orca (Version 5.03)[9] and followed by frequency analysis to ensure that all the molecular configurations have no imaginary frequency. Geometry optimization, single frequency analysis, single point energy were calculated under B3LYP function,[10] and def2-TZVP basis set. Subsequently, the energy decomposition analysis based on SAPT was calculated by using PSI4 package,[11] version 1.4. The energy decomposition contains electrostatic interaction, dispersion

interaction, induction interaction, and exchange repulsion interaction, which was calculated under $SAPT^{2+}(3)\delta MP^2$/aug-cc-pVTZ method. The SAPT script analysis were generated by using Multiwfn program (version: 3.8 dev).[12] All the visualization were done by using VMD (version 1.93).

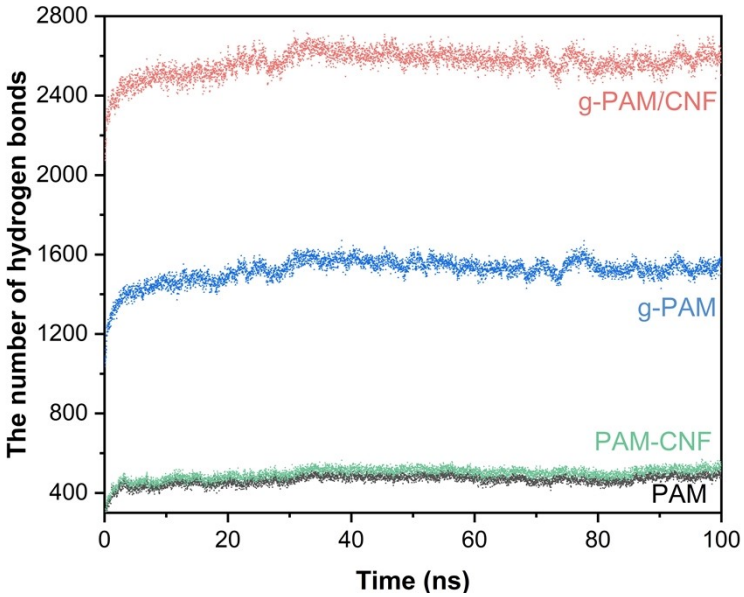

Figure S1. The change of number of hydrogen bonds of varied systems within 100 ns.

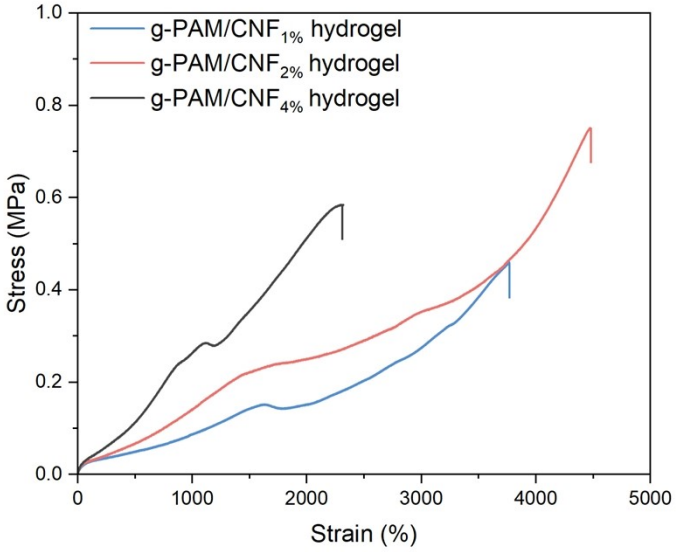

Figure S2. Typical tensile stress-strain curves of g-PAM/CNF hydrogels with varied CNF contents

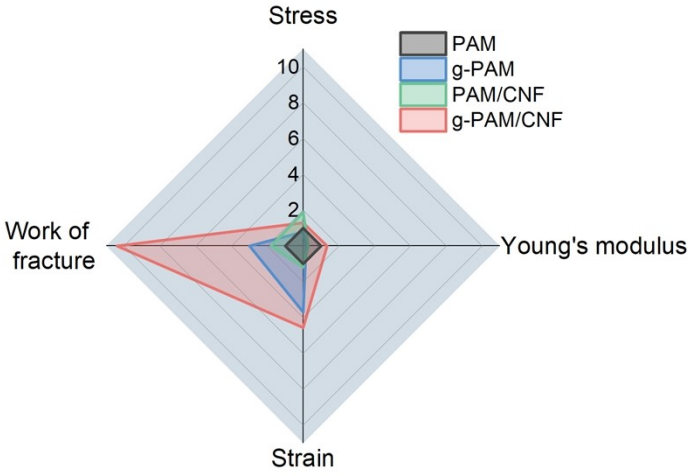

Figure S3. Enhancement factor comparison of different hydrogel systems, using pure PAM hydrogels as reference.

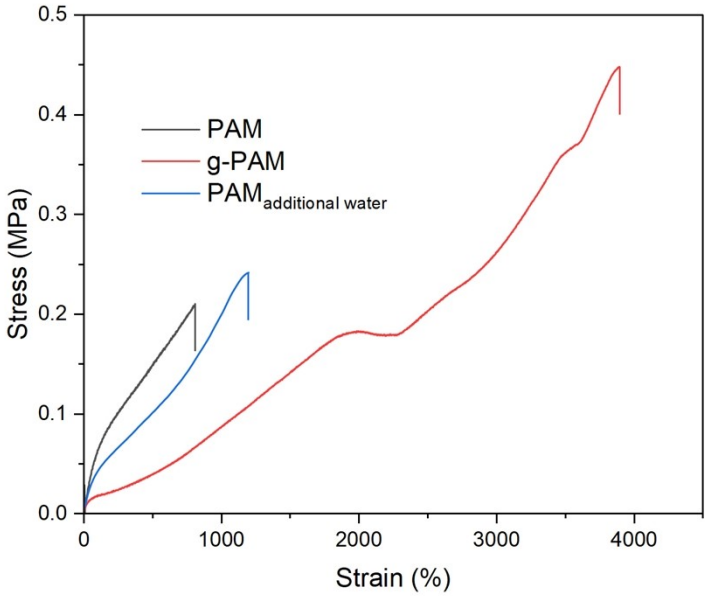

Figure S4. Typical tensile stress-strain curves of hydrogels with varied components.

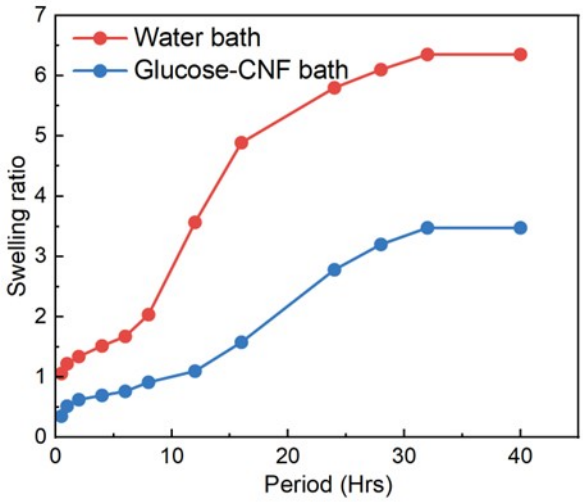

Figure S5. Swelling kinetic curves of PAM hydrogel soaking inside water and glucose/CNF solution bath

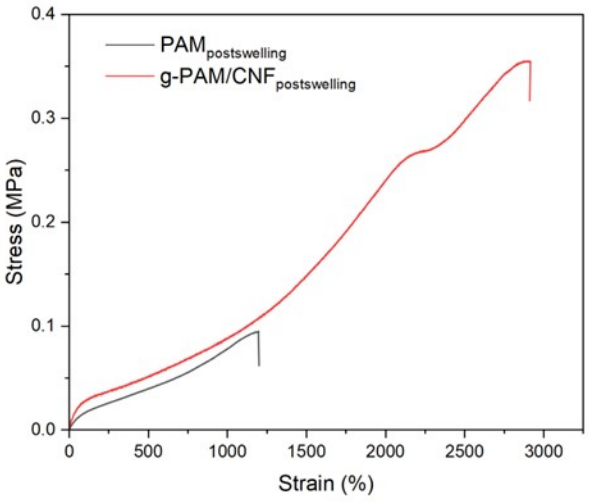

Figure S6. Typical tensile stress-strain curves of hydrogels fabricated by post swelling method.

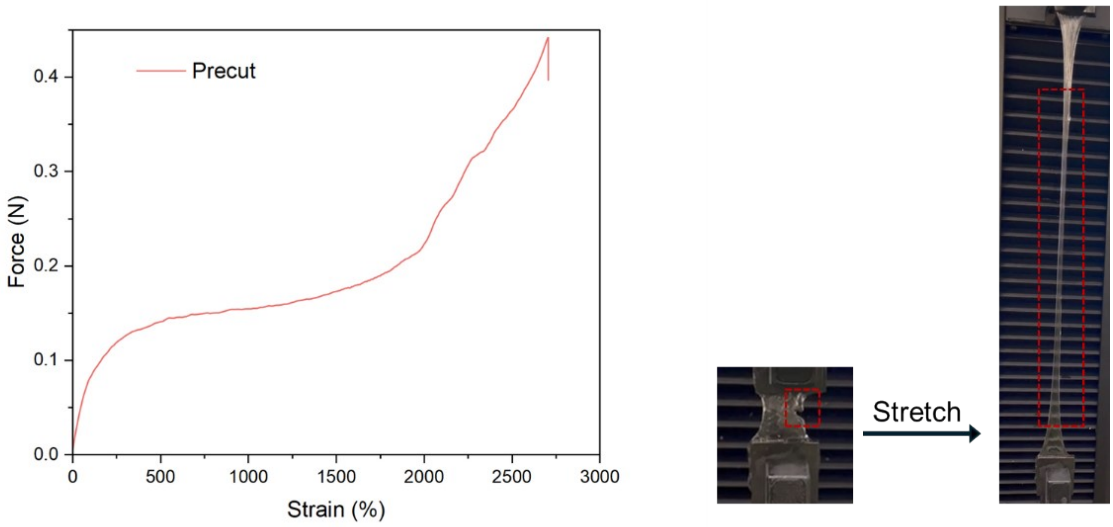

Figure S7. Tensile curve of notched g-PAM/CNF hydrogel sample and testing photo

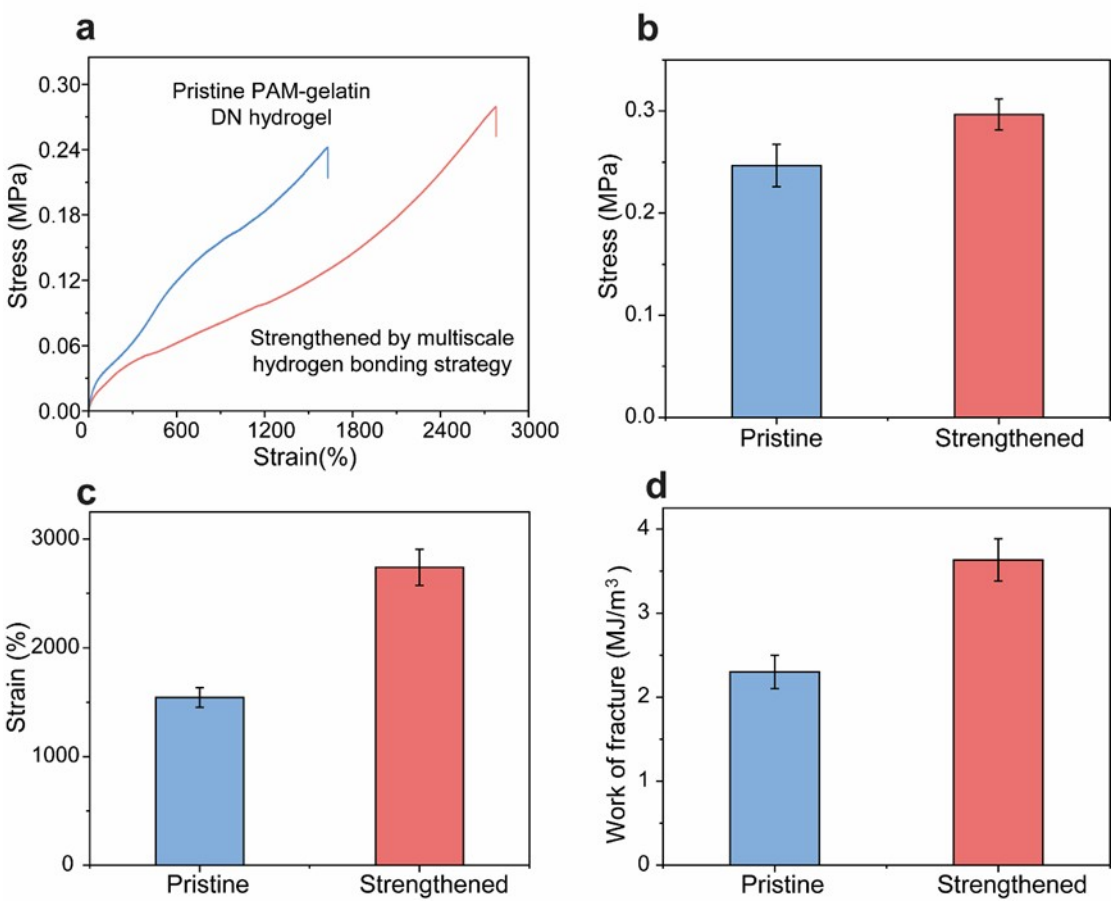

Figure S8. Mechanical properties of pristine PAM-gelatin double network hydrogels and after being strengthened by multiscale hydrogen bonding strategy, including (a) Tensile stress-strain curves; (b) Stress; (c) Strain; and (d) Work of fracture.

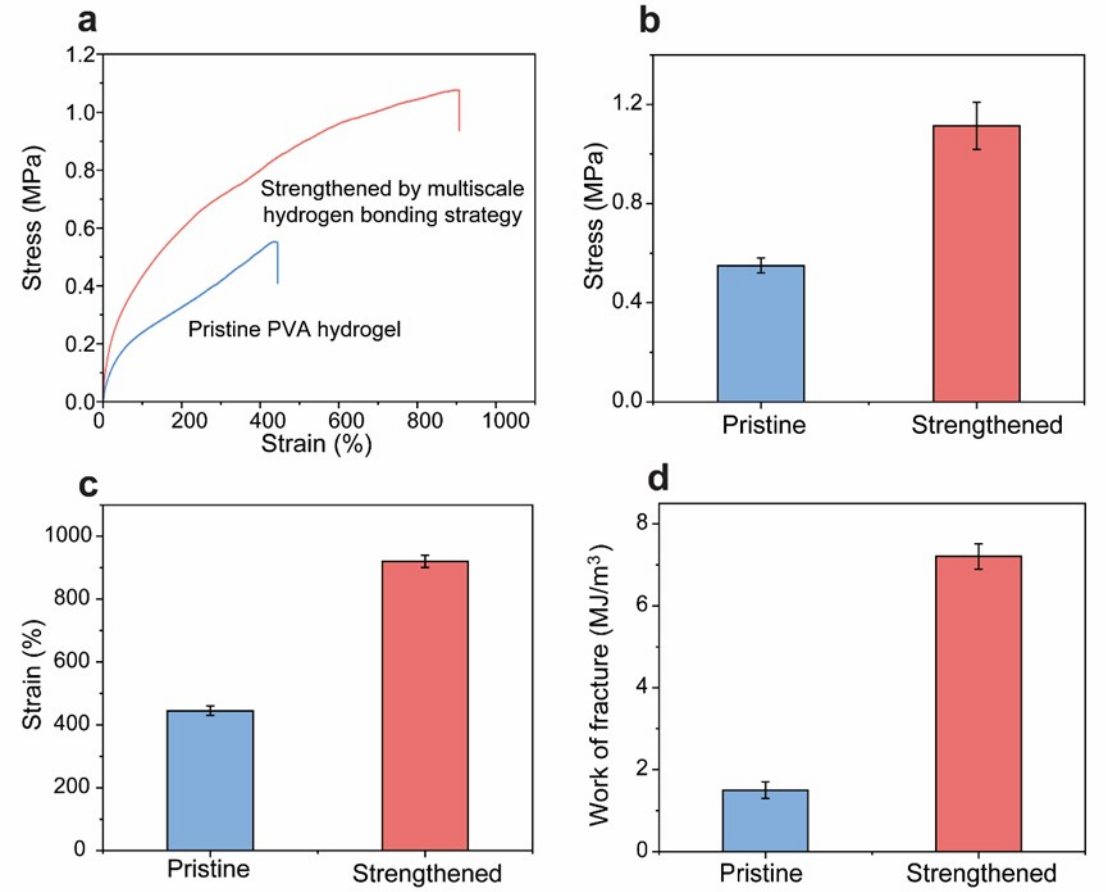

Figure S9. Mechanical properties of pristine PVA hydrogel and after being strengthened by multiscale hydrogen bonding strategy; including (a) Tensile stress-strain curves; (b) Stress; (c) Strain; and (d) Work of fracture.

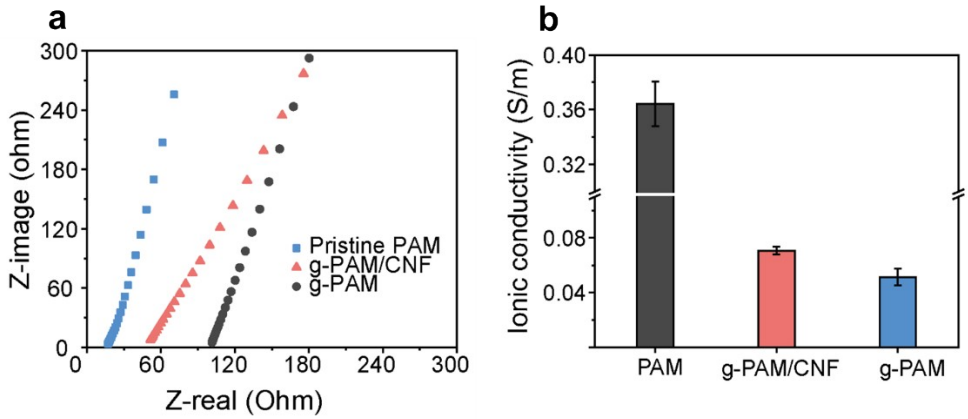

Figure S10. (a) EIS Nyquist curves of varied hydrogel systems and (b) calculated ionic conductivity of different hydrogel systems

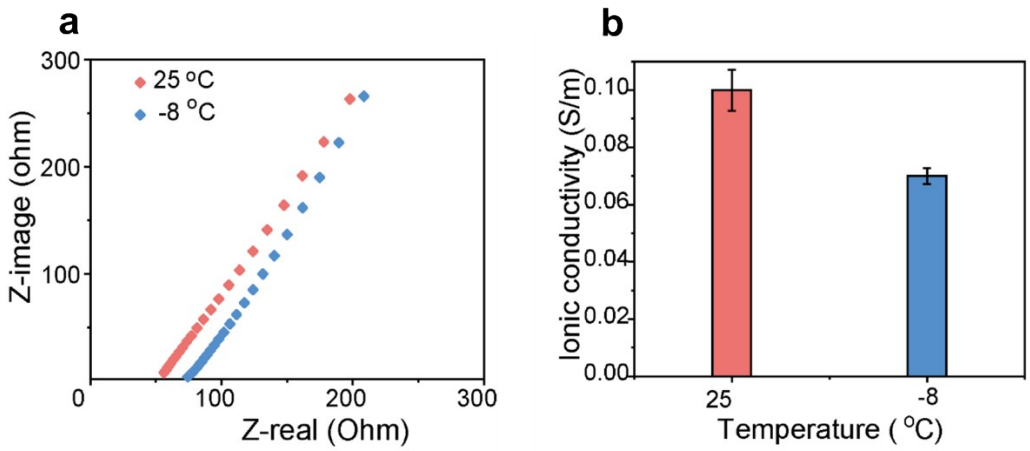

Figure S11. (a) EIS Nyquist curves of g-PAM/CNF hydrogels at 25 and -8 °C (b) ionic conductivity value of g-PAM/CNF hydrogels at 25 and -8 °C

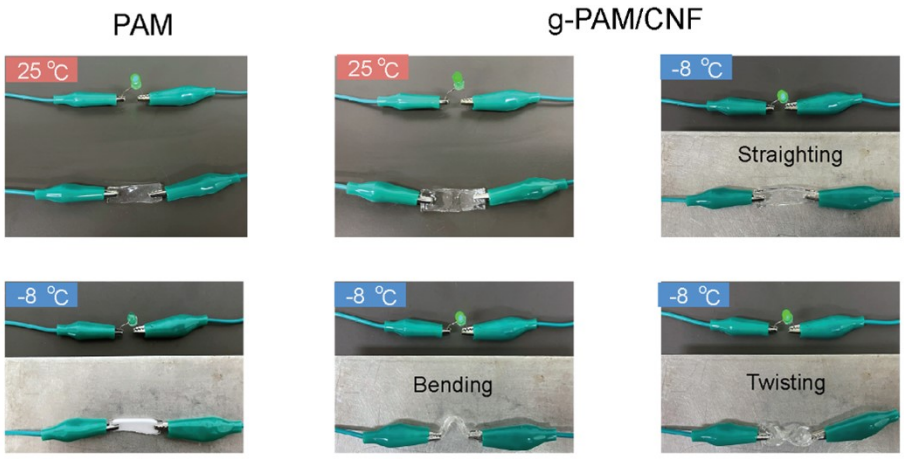

Figure S12. Digital photos presenting the appearance and mechanical properties change for PAM and g-PAM/CNF hydrogels at - 8 ^{o}C;

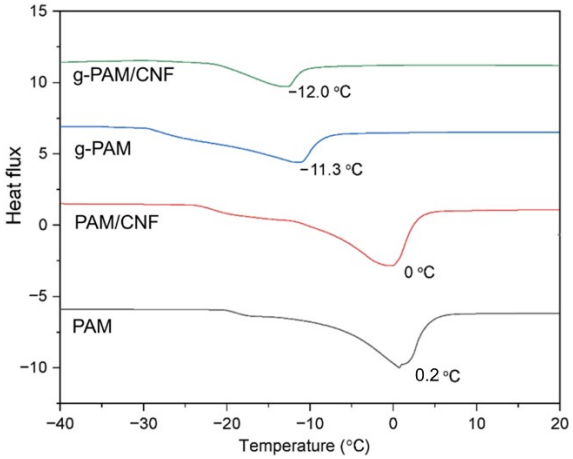

Figure S13. DSC profiles for a series of hydrogel systems

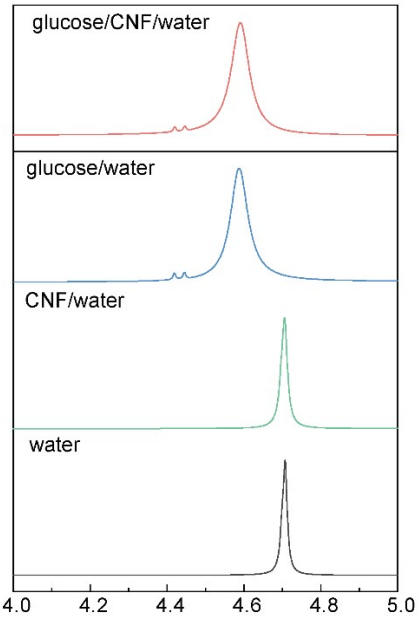

Figure S14. ^{1}H NMR spectra for a series of hydrogel systems

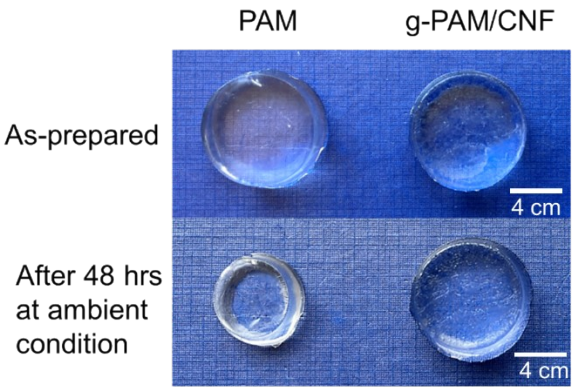

Figure S15. Digital photos demonstrating the appearance change of PAM and g-PAM/CNF hydrogels after being exposed to ambient conditions for 48 hrs

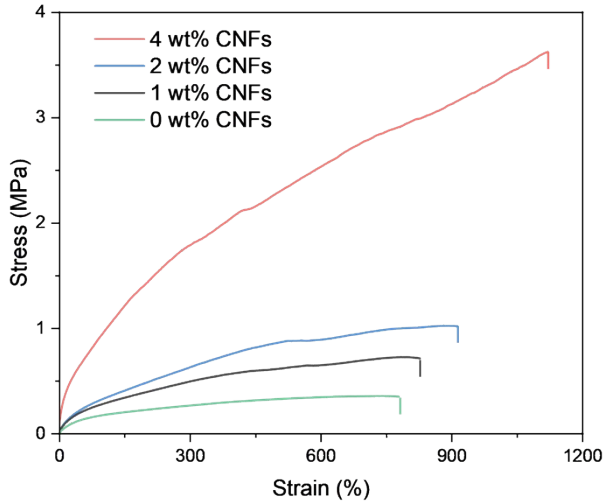

Figure S16. Typical tensile stress-strain curves of g-PAM/CNF alcogels curves with different CNF contents

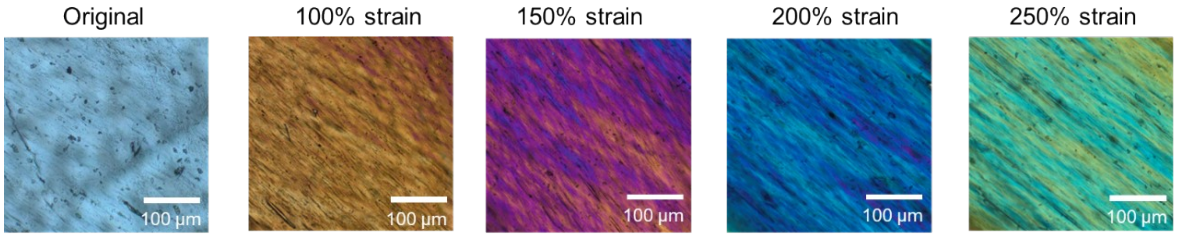

Figure S17. Optical microscopic photos demonstrating the color change of g-PAM/CNF alcogels under different strains (under polarizer)

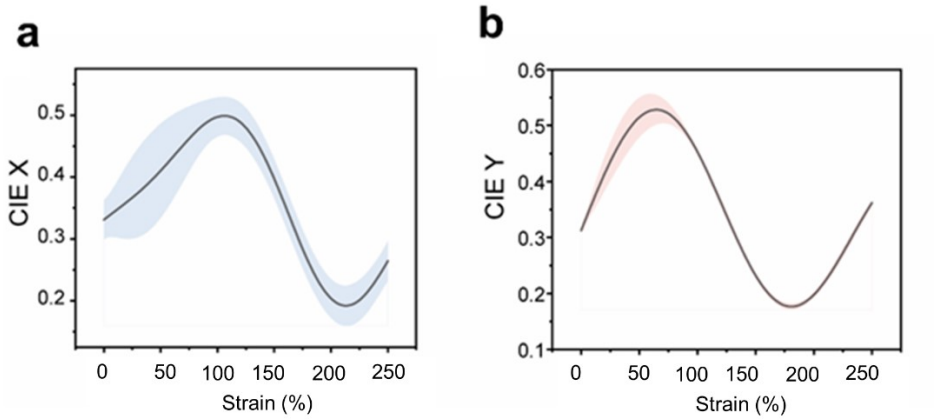

Figure S18 a&b Machine learning models for building continuous relationship among CIE X, Y value, and corresponding strain with specified error bar.

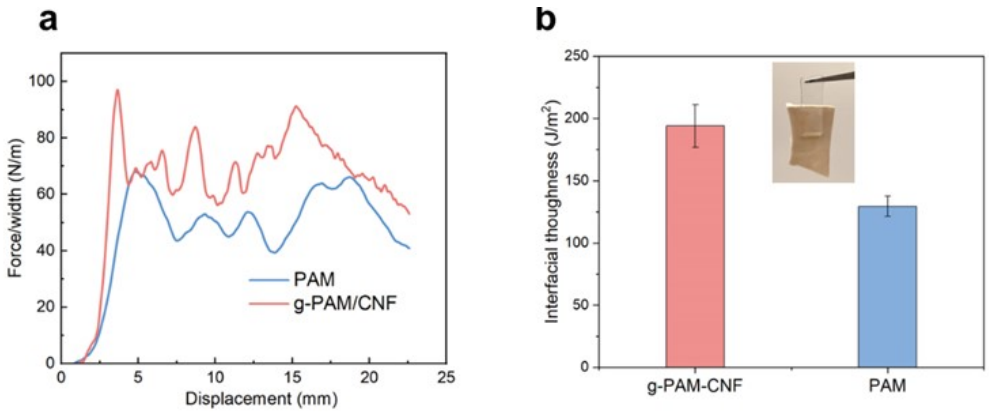

Figure S19. (a) Representative force/width vs. displacement curves for the 180-degree peel tests of various hydrogels; (b) corresponding calculated interfacial toughness value (the inserted photo showing the strong adhesion between g/PAM-CNF hydrogel and porcine skin).

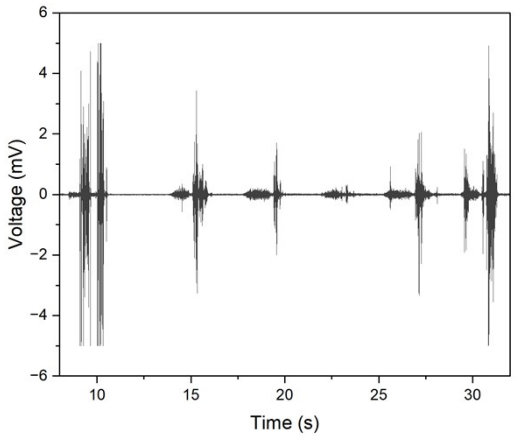

Figure S20. EMG signal recorded by electrodes without hydrogel

Reference

1. Jiang, F., Han, S. & Hsieh, Y. Lo. Controlled defibrillation of rice straw cellulose and self-assembly of cellulose nanofibrils into highly crystalline fibrous materials. *RSC Adv.* **3**, 12366–12375 (2013).
2. Nishiyama, Y., Sugiyama, J., Chanzy, H. & Langan, P. Crystal Structure and Hydrogen Bonding System in Cellulose Iα from Synchrotron X-ray and Neutron Fiber Diffraction. *J. Am. Chem. Soc.* **125**, 14300–14306 (2003).
3. Choi, Y. K. *et al.* CHARMM-GUI Polymer Builder for Modeling and Simulation of Synthetic Polymers. *J. Chem. Theory Comput.* **17**, 2431–2443 (2021).
4. Allouche, A. Software News and Updates Gabedit — A Graphical User Interface for Computational Chemistry Softwares. *J. Comput. Chem.* **32**, 174–182 (2012).
5. William H, Andrew D & Klaus S. VMD - Visual Molecular Dynamics. *J. Mol. Graph.* **14**, 33–38 (1996).
6. Hess, B., Kutzner, C., Van Der Spoel, D. & Lindahl, E. GRGMACS 4: Algorithms for highly efficient, load-balanced, and scalable molecular simulation. *J. Chem. Theory Comput.* **4**, 435–447 (2008).
7. Mark, P. & Nilsson, L. Structure and dynamics of the TIP3P, SPC, and SPC/E water models at 298 K. *J. Phys. Chem. A* **105**, 9954–9960 (2001).
8. Guvench, O. *et al.* CHARMM additive all-atom force field for carbohydrate derivatives and its utility in polysaccharide and carbohydrate-protein modeling. *J. Chem. Theory Comput.* **7**, 3162–3180 (2011).
9. Páll, S. & Hess, B. A flexible algorithm for calculating pair interactions on SIMD architectures. *Comput. Phys. Commun.* **184**, 2641–2650 (2013).
10. Neese, F., Wennmohs, F., Becker, U. & Riplinger, C. The ORCA quantum chemistry program package. *J. Chem. Phys.* **152**, (2020).
11. Weigend, F. & Ahlrichs, R. Balanced basis sets of split valence, triple zeta valence and quadruple zeta valence quality for H to Rn: Design and assessment of accuracy. *Phys. Chem. Chem. Phys.* **7**, 3297–3305 (2005).
12. Lu, T. & Chen, F. Multiwfn: A multifunctional wavefunction analyzer. *J. Comput. Chem.* **33**, 580–592 (2012).